Bistable Helmholtz solitons in cubic-quintic materials

J. M. Christian and G. S. McDonald
Joule Physics Laboratory, School of Computing, Science and Engineering, Institute for Materials Research, University of Salford, Salford M5 4WT, United Kingdom

P. Chamorro-Posada
Departamento de Teoría de la Señal y Comunicaciones e Ingeniería Telemática, Universidad de Valladolid, ETSI Telecomunicación, Campus Miguel Delibes s/n, 47011 Valladolid, Spain

(Received 24 July 2007; published 28 September 2007)

We propose a nonlinear Helmholtz equation for modeling the evolution of broad optical beams in media with a cubic-quintic intensity-dependent refractive index. This type of nonlinearity is appropriate for some semiconductor materials, glasses, and polymers. Exact analytical soliton solutions are presented that describe self-trapped nonparaxial beams propagating at *any* angle with respect to the reference direction. These spatially symmetric solutions are, to the best of our knowledge, the first bistable Helmholtz solitons to be derived. Accompanying conservation laws (both integral and particular forms) are also reported. Numerical simulations investigate the stability of the solitons, which appear to be remarkably robust against perturbations.

DOI: 10.1103/PhysRevA.76.033833 PACS number(s): 42.65.Tg, 42.65.Wi, 42.70.−a, 42.79.−e

I. INTRODUCTION

Solitons are universal, self-localizing, and self-stabilizing waves that may exist in systems where linear effects are opposed by nonlinearity [1]. In optics, spatial solitons can become dominant electromagnetic modes if the diffraction of a beam propagating through a nonlinear medium is balanced by locally induced refractive-index changes [2–4]. Investigations of spatial solitons often involve planar waveguiding structures that comprise a longitudinal dimension and a single effective transverse dimension. In uniform media, these two directions are physically equivalent. The robustness of spatial solitons against perturbations means that they could be used as elementary information units, or "bits" in future Information Communication and Technology (ICT) all-optical devices. Applications as diverse as induced waveguiding [5], switching in scalar [6] and vector [7] regimes, optical memory [8], and computing with solitons [9] have been proposed. The bistable operation of such devices is likely to be a key consideration.

In his seminal paper, Kaplan showed that generic evolution equations sometimes support bistable solitons [10]. Bistable (multistable) solutions are possible when the beam power becomes a double-valued (multivalued) function of an internal parameter, such as the propagation constant. This type of bistability is *intrinsic*, meaning that it arises solely from the interplay between light and the host medium. Crucially, no feedback mechanism, e.g., from cavity mirrors or interfaces (see Ref. [11], and references therein), is required. According to Kaplan's framework, multistability requires the nonlinear refractive-index function $n_{NL}(I)$, where I is the local beam intensity, to have either a change in sign, or a sufficiently sharp peak in its derivative dn_{NL}/dI. These conditions rule out Kerr-type media, where $n_{NL}(I) \propto I$, for supporting intrinsically multistable states. Optical devices that specifically exploit instrinsically bistable solitons therefore require host materials with appreciable higher-order nonlinear susceptibilities [12–14].

Gatz and Herrmann have studied a type of intrinsic bistability [15–17] that is distinct from Kaplan's bistability [10–14]. They considered a bright soliton of an evolution equation where the peak intensity (as opposed to the beam power) may be a double-valued function of a (normalized) control parameter that characterizes the material nonlinearity. The result is a pair of coexisting solutions with different peak intensities, but the same full-width-at-half-maximum (FWHM) values.

An extensive body of research on bistable solitons has developed in the literature over recent years. The few works cited above, for example, have provided a huge amount of insight into optical systems where the governing equation is of the nonlinear Schrödinger (NLS) class [8,10–18]. Diffraction in these models is paraxial, occurring in one dimension only (transversely to a single reference direction). Here, we consider regimes involving bistability where the governing equation is of the nonlinear Helmholtz (NLH) class, and diffraction is thus fully two dimensional. By folding the phenomenon and formalism of multistability into Helmholtz soliton theory, one can model bistable spatial solitons in a wide range of angular contexts.

We consider a medium with a cubic-quintic nonlinear refractive index $n_{NL}(I)=n_2 I+n_4 I^2$, where n_2 is the Kerr coefficient and n_4 parametrizes a quintic correction term. This classic model [19] is advantageous for two main reasons. First, it is a relatively simple generalization of the Kerr response and permits exact analytical soliton solutions to be derived. Second, cubic-quintic media are readily available, so we expect our predictions to be directly observable in the laboratory. Many different optical materials have a refractive index that can be well described by a cubic-quintic nonlinearity. Examples include some semiconductors and doped glasses, such as AlGaAs [20] and CdS_xSe_{1-x} [21,22], respectively, the polydiacetylene *para*-toluene sulfonate (or "PTS") π-conjugated polymer [23–25], chalcogenide glasses (e.g., Ag-As-Se systems) [26–28], and some transparent organic materials [29]. A nonlinearity with competing cubic and

quintic contributions also provides a generic model for saturation [30] in, for instance, double-doped materials [31,32].

The layout of this paper is as follows. In Sec. II, we review the limitations of modeling optical beams within the paraxial approximation. Ultranarrow-beam and Helmholtz nonparaxial scenarios are defined, and their key physical and mathematical differences are detailed. In Sec. III, the exact analytical bistable Helmholtz solitons are presented and their geometrical properties are explored in detail. We also give a complete account of the regime and character of both paraxial and Helmholtz bistable solutions, generalizing previous analyses [17] to much wider parameter ranges. General and particular forms for three conservation laws are also reported. In a multiple limit, well-known paraxial solitons are shown to emerge from the Helmholtz generalizations. In Sec. IV, the stability of the solutions is tested using numerical perturbative methods. We conclude, in Sec. V, with some remarks about the usefulness of Helmholtz soliton theory in relation to modeling future optical devices.

II. NONPARAXIAL MODELS

Paraxial propagation models remain valid so long as the beams they describe are (i) broad compared to their carrier wavelength, (ii) moderately intense, and (iii) evolving along (or at negligible angles with respect to) the reference direction. If all three of these criteria are not met simultaneously, then propagation is, by definition, *nonparaxial*.

Since the groundbreaking work of Lax *et al.* [33], many authors have considered ultranarrow-beam (or subwavelength) nonparaxiality, where only condition (i) is violated [34–44]. It is now well known that the vector nature of the electric field plays a central role when the waist w_0 of an optical beam becomes comparable to its (free-space) carrier wavelength λ. This particular nonparaxial context is relevant to the *miniaturization* aspect of ICT applications, where the physical size of the device tends toward λ. Descriptions of ultranarrow beams are routinely based upon the assumption of a single parameter of smallness, $\varepsilon \equiv \lambda / w_0$. When $\varepsilon \sim O(1)$, strong coupling between the transverse and longitudinal field components leads to appreciable divergence in the nonlinear polarization. An order-of-magnitude analysis of Maxwell's equations, up to $O(\varepsilon^2)$, can then yield a wave equation for the dominant (transverse) component. The basic structure of this equation is typically of the NLS type, supplemented by a range of higher-order and nonlinear diffractive terms.

The Helmholtz nonparaxial scenario is defined by the relaxation of condition (iii) alone, so that only broad beams of moderate intensity are considered [45]. In this regime, ultranarrow-beam modifications are unimportant because $\varepsilon \ll O(1)$ is always rigorously satisfied. The electric field may be taken as being purely transverse (typically TE polarized), and the refractive-index distribution can be described within the scalar approximation. The angular restriction of paraxial models can be avoided if one omits the slowly varying envelope approximation [46,47], thereby preserving the full generality of the bidirectional governing equation. Bidirectionality permits both forward and backward propagation, hence beams are allowed to evolve and interact at any angle with respect to the reference direction [48].

A physical subtlety overlooked by paraxial theory is that the properties of a system must not depend upon the orientation of the observer's coordinate axes. For instance, if a beam is stable when it propagates in the reference direction, then the same beam must also be stable when the coordinate axes are rotated through an arbitrary angle. It is also clear that, in uniform media, instability cannot arise from a rotational transformation because all such frames are physically indistinguishable. Helmholtz diffraction [49] respects this spatial symmetry.

Off-axis effects can be eliminated for a single isolated beam through a convenient alignment of the coordinate axes. However, even the simplest experimental configurations can generally preclude the existence of a unique reference direction. Optical arrangements involving, for example, multiplexing [50] and the oblique incidence of beams at material interfaces [51] have intrinsically angular characters that cannot be accessed by paraxial models. We have recently reanalyzed these two elementary geometries for Kerr nonlinearities using Helmholtz soliton theory [52,53]. New qualitative phenomena were predicted, and corrections to paraxial theory easily exceeding 100% were uncovered.

III. HELMHOLTZ SOLITONS

A. Model equation

We consider a continuous-wave TE-polarized electric field with angular frequency ω,

$$\tilde{E}(x,z,t) = E(x,z)\exp(-i\omega t) + E^*(x,z)\exp(+i\omega t). \quad (1)$$

If the complex envelope modulating the carrier oscillations varies on a scale length much larger than λ, then $E(x,z)$ satisfies

$$\left(\frac{\partial^2}{\partial z^2} + \frac{\partial^2}{\partial x^2}\right)E(x,z) + \frac{\omega^2}{c^2}n^2(|E|^2)E(x,z) = 0. \quad (2)$$

The spatial coordinates appear symmetrically in Eq. (2) so that diffraction occurs in both x and z directions [45,46]. A cubic-quintic nonlinearity is introduced through the scalar refractive index distribution $n(|E|^2)=n_0+n_{NL}(|E|^2)$, where n_0 is the linear index and $n_{NL}(|E|^2)=n_2|E|^2+n_4|E|^4$ is the field-dependent part. The Kerr coefficient is taken to be positive (i.e., $n_2>0$), but n_4 may assume positive or negative values. For weak optical nonlinearities, one has that $|n_{NL}| \ll n_0$ so, to an excellent approximation, $n^2(|E|^2) \simeq n_0^2 + 2n_0 n_{NL}(|E|^2)$. To facilitate a comparison between Helmholtz and conventional (paraxial) models, the z axis is chosen as the reference direction and the spatial part of the electric field is expressed as $E(x,z)=E_0 u(x,z)\exp(ikz)$, where $k=n_0 k_0$ and $k_0 \equiv \omega/c = 2\pi/\lambda$. By substituting this into Eq. (2), one may derive, without further approximation, a governing equation for the dimensionless envelope u,

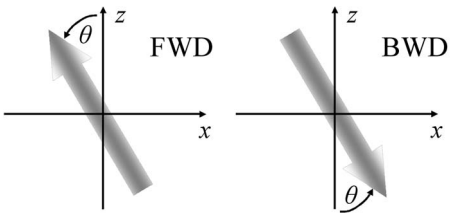

FIG. 1. Schematic diagram illustrating the forward (FWD) and backward (BWD) solitons of Eqs. (4). The FWD and BWD solutions are essentially indistinguishable, as they must be, since whether evolution occurs in the "forward" or 'backward' direction depends solely upon the relative orientation of the observer's coordinate axes with respect to the beam. x and z are the laboratory or physical coordinates (schematically represented in the same unscaled units). The angles marked in the figure denote the sense of the propagation angle $\theta>0$.

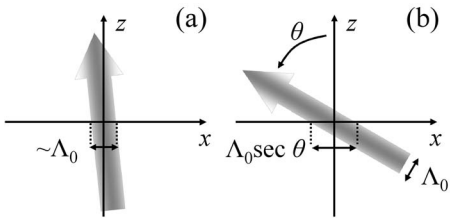

FIG. 2. Schematic diagram (to scale) illustrating the angular beam broadening effect. Beams are plotted in the laboratory or unscaled (x,z) frame, and the coordinates are in the same units (determined by the choice of the beam widths). Part (a) shows a quasiparaxial ($\theta=6°$) configuration, and part (b) shows a typical Helmholtz ($\theta=60°$) regime. In (a), propagation is constrained to be very nearly along the z axis, in which case geometrical broadening is negligible. In (b), evolution at a finite angle can lead to an arbitrarily large increase in the beam width as $\theta\to\pm 90°$.

$$\kappa\frac{\partial^2 u}{\partial\zeta^2}+i\frac{\partial u}{\partial\zeta}+\frac{1}{2}\frac{\partial^2 u}{\partial\xi^2}+|u|^2u+\alpha|u|^4u=0. \tag{3}$$

$\xi=\sqrt{2}x/w_0$ and $\zeta=z/L_D$ are the dimensionless spatial coordinates, normalized with respect to a reference Gaussian beam of waist w_0 and diffraction length $L_D=kw_0^2/2$. The electric field is measured in units of $E_0\equiv(n_0/kn_2L_D)^{1/2}$, while $\kappa=1/k^2w_0^2\equiv\varepsilon^2/4\pi^2n_0^2\ll O(1)$ quantifies the (inverse) beam width and $\alpha\equiv E_0^2n_4/n_2$ parametrizes the ratio of the quintic to the cubic nonlinear phases for the input beam. $\alpha>0$ when $n_4>0$ (focusing quintic nonlinearity) and $\alpha<0$ when $n_4<0$ (defocusing quintic nonlinearity).

B. Exact bright solitons

We have derived the following exact analytical bright solitons of Eq. (3):

$$u(\xi,\zeta)=\rho^{1/2}(\xi,\zeta)\exp\left[i\sqrt{\frac{1+4\kappa\beta}{1+2\kappa V^2}}\left(\mp V\xi\pm\frac{\zeta}{2\kappa}\right)\right]\times\exp\left(-i\frac{\zeta}{2\kappa}\right), \tag{4a}$$

$$\rho(\xi,\zeta)=\frac{4\beta}{1+\left(1+\frac{4}{3}\alpha\rho_0\right)\cosh[\Theta(\xi,\zeta)]}, \tag{4b}$$

$$\Theta(\xi,\zeta)=2(2\beta)^{1/2}\frac{\xi\pm V\zeta}{\sqrt{1+2\kappa V^2}}, \tag{4c}$$

$$\beta\equiv\beta(\alpha,\rho_0)=\frac{\rho_0}{2}\left(1+\frac{2}{3}\alpha\rho_0\right), \tag{4d}$$

and ρ_0 is the peak intensity. The forward (backward) solution in Eqs. (4) corresponds to the upper (lower) choice of signs. Equations (4) describe an exponentially localized beam propagating at an angle $\theta=\tan^{-1}(\sqrt{2\kappa}V)$ relative to the $+z$ $(-z)$ axis, where V is the transverse velocity parameter and $-90°\leqslant\theta\leqslant+90°$ (see Fig. 1). It is important to note that there is no physical distinction between the forward and backward beams. This follows from the fact that the "forward" and "backward" designations are only meaningful once the (x,z) coordinate axes have been defined. The equivalence of the two solutions in Eqs. (4) can be established mathematically by combining them, through trigonometric identity, into

$$u(\xi,\zeta)=\rho^{1/2}(\xi,\zeta)\exp\left[i\sqrt{\frac{1+4\kappa\beta}{2\kappa}}\left(-\xi\sin\theta+\frac{\zeta}{\sqrt{2\kappa}}\cos\theta\right)\right]\exp\left(-i\frac{\zeta}{2\kappa}\right), \tag{5a}$$

$$\Theta(\xi,\zeta)=2(2\beta)^{1/2}\left(\xi\cos\theta+\frac{\zeta}{\sqrt{2\kappa}}\sin\theta\right). \tag{5b}$$

Thus, by eliminating the transverse velocity parameter, it can be seen that there is really just a single beam that may propagate at *any* angle, $-180°\leqslant\theta\leqslant+180°$, with respect to the $+z$ direction.

Solutions (4) include all the generic features of Helmholtz solitons [45–48,54–57], including the longitudinal phase factor $\exp(-ikz)$, and angular and intensity-dependent modifications to the beam wave vector. Spatial symmetry also leads to geometrical beam broadening. During oblique evolution, an observer in the (x,z) coordinate frame perceives the beam width to be increased by a factor of $(1+2\kappa V^2)^{1/2}=\sec\theta$ relative to its on-axis value (see Fig. 2). This effect is negligible for paraxial angles (which are implicitly tiny), but it becomes entirely nontrivial at moderate and large angles. For example, when $\theta=\pm 60°$, one finds that $2\kappa V^2=3$, irrespective of κ, and the beam width is increased by a factor of 2. In the extreme cases of $\theta=\pm 90°$, where propagation is along the $\mp x$ axis, one has that $2\kappa V^2\to\infty$ and the Helmholtz soliton (4) becomes,

$$u(\xi,\zeta)=\rho^{1/2}(\zeta)\exp\left[\mp i\sqrt{\frac{1+4\kappa\beta}{2\kappa}}\xi\right]\exp\left(-i\frac{\zeta}{2\kappa}\right), \tag{6a}$$

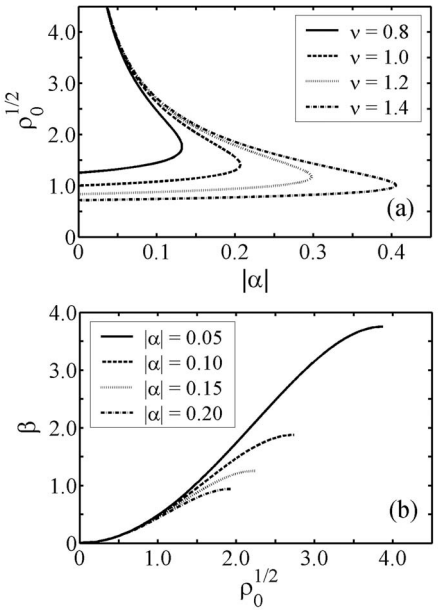

FIG. 3. (a) Bistable solution families for several values of ν, obtained by solving Eq. (7). For fixed $|\alpha|$ and ν, solitons residing on the two branches have different peak intensities ρ_0, but the same full-width-half-maximum values. The dashed line, corresponding to $\nu=1$, was presented in Ref. [17]. (b) Dependence of the parameter β on ρ_0 [see Eq. (4d)].

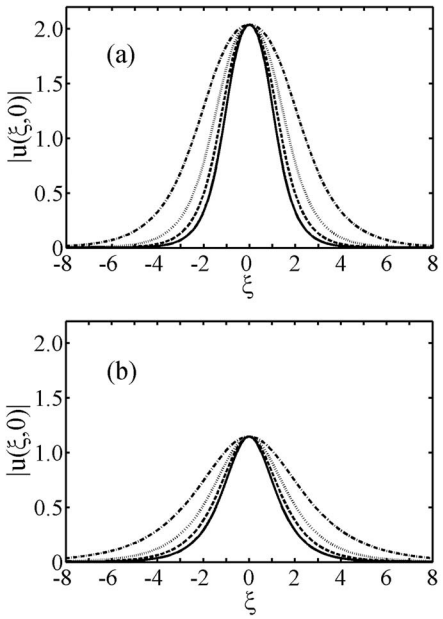

FIG. 4. Helmholtz soliton profiles for (a) upper-, and (b) lower-branch solutions with $\nu=1$ and $\alpha=-0.15$. From Fig. 3(b), the peak amplitudes are $\sqrt{\rho_0}\approx 2.03$ and $\sqrt{\rho_0}\approx 1.14$, respectively. Propagation angles are $\theta=0°$ (solid line), $\theta=30°$ (dashed line), $\theta=45°$ (dotted line), and $\theta=60°$ (dot-dashed line). Solid lines coincide with exact paraxial solution (12), where no broadening is present.

$$\Theta(\zeta) = 2(2\beta)^{1/2}\frac{\zeta}{\sqrt{2\kappa}}. \tag{6b}$$

The beam thus appears to be infinitely broad when viewed from the (x,z) frame since it is evolving perpendicularly to the z axis.

$\kappa\partial_{\zeta\zeta}$ is a fundamental part of the linear wave operator in Eq. (3). Its geometrical contribution $2\kappa V^2$ is unbounded, even when $\kappa \simeq 0$, and is independent of system nonlinearity. These results demonstrate that potentially dominant Helmholtz angular effects cannot be quantified by the single-parameter (i.e., κ-based) expansions routinely deployed in ultranarrow-beam analyses [34–44]. They also suggest that $\kappa\partial_{\zeta\zeta}$ should not generally be regarded as a small, e.g., $O(\kappa)$, perturbation [1,58–60] to a paraxial governing equation [17].

C. Bistable solutions

Insight into the bistable character of solution (4) can be gained by considering a half-width intensity distribution, which is defined by the condition $|u(s)|^2=\frac{1}{2}\rho_0$. Here, $s=|\xi \pm V\zeta|(1+2\kappa V^2)^{-1/2} \equiv \nu\Delta$ denotes the half-width, $\Delta \equiv \mathrm{sech}^{-1}(2^{-1/2}) \approx 0.88$, and the parameter $\nu>0$ is introduced to determine the half-width of the beam in units of Δ. This condition leads to the transcendental equation for ρ_0,

$$\rho_0^{1/2} = \left(\frac{1}{2\nu\Delta}\right)\frac{1}{\sqrt{1+\frac{2}{3}\alpha\rho_0}}\cosh^{-1}\left(\frac{3+\frac{8}{3}\alpha\rho_0}{1+\frac{4}{3}\alpha\rho_0}\right). \tag{7}$$

Gatz and Herrmann [17] studied the canonical solutions of Eq. (7), defined by $\nu=1$. Solitons in this solution subset have half-widths of $s=\Delta$. When $|\alpha|\to 0$, one then recovers the unit-amplitude Kerr bright soliton, where $\rho_0^{1/2}=1$. We now show that there exist much broader classes of bistable solution families that are characterized by a continuum of values of ν.

When $\alpha>0$, there is a unique value of ρ_0 that satisfies Eq. (7), for each soliton width. The situation is more interesting when $\alpha<0$. The curves in Fig. 3(a) reveal that for each choice of ν, there are generally two distinct values of ρ_0 that satisfy Eq. (7) within some finite interval $0<|\alpha|<|\alpha|_{\mathrm{crit}}$, where $|\alpha|_{\mathrm{crit}}$ is a cutoff. These roots characterize a pair of beams with different peak intensities but that, by definition, possess the same FWHM, given by $2\nu\Delta$. As $|\alpha|\to 0$, the upper branch diverges toward infinity while the lower branch tends to $\rho_0^{1/2}\sim 1/\nu$.

Inspection of the general solution (4) shows that when $\alpha<0$, the peak intensity is constrained by $|\alpha|\rho_{0\max}=3/4$. The divergence of the upper branches in Fig. 3(a) occurs as this limit is approached. Each pair of particular bistable solitons (for fixed $|\alpha|$) shown in Fig. 3(a) corresponds to a pair of points on the curves given in Fig. 3(b). Note also that since there is a maximum allowed peak intensity for each $|\alpha|$, there is a corresponding maximum allowed β, which is given by $\beta_{\max}=\rho_{0\max}/4$. Beam profiles for canonical solitons, including the angular broadening effect, are shown in Fig. 4.

The bistability properties of Helmholtz solitons do not depend upon the propagation angle, even though other beam parameters depend strongly on this angle. Such an intuitive result could have been predicted *a priori* on the grounds of rotational symmetry. The independence of ρ_0 with respect to θ follows directly from the fact that the FWHM is measured

in the direction *transverse* to the propagation axis, and is therefore uniquely determined for a given beam. It is for this reason that κ and $2\kappa V^2$ corrections do not appear in Eq. (7).

D. Conservation laws

Noether's theorem connects the conservation laws of a continuous system to its symmetries through a quite general field-theoretic prescription [61]. Model (3) and its complex conjugate can be regarded as Euler-Lagrange equations for a Lagrangian density L (i.e., $\delta L/\delta u^*=0$ and $\delta L/\delta u=0$, respectively, where $\delta/\delta u$ and $\delta/\delta u^*$ denote variational derivatives). With L given by

$$L=\frac{i}{2}\left(u^*\frac{\partial u}{\partial\zeta}-u\frac{\partial u^*}{\partial\zeta}\right)-\kappa\frac{\partial u}{\partial\zeta}\frac{\partial u^*}{\partial\zeta}-\frac{1}{2}\frac{\partial u}{\partial\xi}\frac{\partial u^*}{\partial\xi}+\frac{1}{2}|u|^4+\frac{1}{3}\alpha|u|^6, \tag{8}$$

one may define a pair of canonically conjugate momentum variables,

$$\pi\equiv\frac{\partial L}{\partial u_\zeta}=-\left(\frac{i}{2}+\kappa\frac{\partial}{\partial\zeta}\right)u^* \tag{9a}$$

and

$$\tilde{\pi}\equiv\frac{\partial L}{\partial u_\zeta^*}=\left(\frac{i}{2}-\kappa\frac{\partial}{\partial\zeta}\right)u. \tag{9b}$$

Here, $u_\zeta\equiv\partial_\zeta u$, etc., and ξ and ζ play the roles of "space" and "time" coordinates, respectively. Three conserved quantities, identified as the energy flow W, the linear momentum M, and the Hamiltonian H, may then be derived as follows:

$$W=\int_{-\infty}^{+\infty}d\xi\left[|u|^2-i\kappa\left(u^*\frac{\partial u}{\partial\zeta}-u\frac{\partial u^*}{\partial\zeta}\right)\right], \tag{10a}$$

$$M=\int_{-\infty}^{+\infty}d\xi\left[\frac{i}{2}\left(u^*\frac{\partial u}{\partial\xi}-\frac{\partial u^*}{\partial\xi}u\right)-\kappa\left(\frac{\partial u^*}{\partial\zeta}\frac{\partial u}{\partial\xi}+\frac{\partial u^*}{\partial\xi}\frac{\partial u}{\partial\zeta}\right)\right], \tag{10b}$$

and

$$H=\int_{-\infty}^{+\infty}d\xi\left[\frac{1}{2}\frac{\partial u}{\partial\xi}\frac{\partial u^*}{\partial\xi}-\kappa\frac{\partial u}{\partial\zeta}\frac{\partial u^*}{\partial\zeta}-\frac{1}{2}|u|^4-\frac{1}{3}\alpha|u|^6\right]. \tag{10c}$$

These integrals arise from the invariance of the field equations under a set of one-parameter infinitesimal transformations (a global phase transformation, and translations in ξ and ζ, respectively). Conservation laws are of fundamental physical and mathematical importance and, in this instance, they are also useful for monitoring the integrity of the numerical scheme [62] used to solve Eq. (3).

Exact algebraic expressions for the invariants can be obtained by substituting solution (4) into integrals (10), whereupon one finds, for the forward soliton,

$$W=(1+4\kappa\beta)^{1/2}P, \tag{11a}$$

$$M=\frac{V}{\sqrt{1+2\kappa V^2}}[(1+4\kappa\beta)P-2\kappa Q], \tag{11b}$$

$$H=\frac{(1+4\kappa\beta)^{1/2}}{2\kappa}P-\frac{M}{2\kappa V}. \tag{11c}$$

When $\alpha>0$, the functions P and Q are given by

$$P\equiv\left(\frac{3}{2\alpha}\right)^{1/2}\tan^{-1}\left(\sqrt{\frac{16\alpha\beta}{3}}\right), \tag{11d}$$

and

$$Q\equiv\frac{1}{2}\left(\frac{3}{8\alpha}\right)\left[\left(1+\frac{16\alpha\beta}{3}\right)P-\sqrt{8\beta}\right]. \tag{11e}$$

One can obtain expressions for P and Q when $\alpha<0$ by making the transformation $\alpha\to-|\alpha|$ in Eqs. (11d) and (11e), in which case

$$P\equiv\left(\frac{3}{2|\alpha|}\right)^{1/2}\tanh^{-1}\left(\sqrt{\frac{16|\alpha|\beta}{3}}\right), \tag{11f}$$

and

$$Q\equiv\frac{1}{2}\left(\frac{3}{8|\alpha|}\right)\left[\sqrt{8\beta}-\left(1-\frac{16|\alpha|\beta}{3}\right)P\right]. \tag{11g}$$

From Eqs. (11b) and (11c), it can be shown that $\partial H/\partial M=\partial_V H/\partial_V M=V$, where ∂_V denotes differentiation with respect to the velocity V. Further analysis has revealed that such a connection between H and M is an intrinsic property of forward Helmholtz bright solitons.

E. Paraxial limit of Helmholtz solitons

Any Helmholtz soliton should converge to its paraxial counterpart whenever the beam behaves paraxially [45–48,54–57]. However, this type of recovery is subtle and cannot be achieved by setting $\kappa=0$. Inspection of Eqs. (4) and (5) shows that such a simple approach would be problematic; one actually requires all contributions from $\kappa\partial_{\zeta\zeta}$ to be negligible simultaneously. A paraxial solution emerges if and only if $\kappa\to0$ (broad beam), $\kappa\rho_0\to0$ (moderate intensity), and $\kappa V^2\to0$ (negligible propagation angle, and thus strictly $\theta\to0°$). By applying this multiple limit to the forward beam in Eqs. (4), one finds that

$$u(\xi,\zeta)\simeq\rho^{1/2}(\xi,\zeta)\exp\left[-iV\xi+i\left(\beta-\frac{V^2}{2}\right)\zeta\right], \tag{12a}$$

and

$$\Theta(\xi,\zeta)\simeq2(2\beta)^{1/2}(\xi+V\zeta), \tag{12b}$$

which is Herrmann's paraxial soliton [17]. It is interesting to note that $\kappa V^2\to0$ can also be satisfied when $\theta\to\pm180°$, where propagation coincides with the $-z$ axis. Such a regime is outside the scope of (unidirectional) paraxial theory, which has no analog of Helmholtz backward waves. Finally, by applying the paraxial limit to the forward conserved quantities, Eqs. (11), one obtains $W\simeq P$ and $M\simeq VP$, and

$$H\simeq\frac{1}{2}V^2P-\beta P+Q. \tag{13}$$

These approximate expressions correspond to the three invariants reported by Gatz and Herrmann [17]. Akhmediev *et*

al. [63] have also considered the paraxial beam power P and the on-axis (i.e., $V=0$) Hamiltonian in Eq. (13) for $\alpha<0$. We stress that solitons lying on the two branches are associated with different values of β and thus, from Eq. (11f), have different beam powers. This confirms that the type of intrinsic bistability discussed in Sec. III C is physically distinct from that discovered by Kaplan [10–14].

IV. SOLITON STABILITY

The stable propagation of beam solutions in elliptic models has been known for several years. For example, a spatial symmetry-preserving algorithm was derived to integrate Eq. (3) numerically [62]. Several previous works have reported that Helmholtz solitons are generally robust entities that are surrounded by wide basins of attraction [48,52–57]. Linear analysis has also established the modulational stability properties of plane-wave solutions to generic NLH equations [55]. Finally, we have found excellent agreement between the predictions of models such as Eq. (3), and direct integration of the fully nonlinear Maxwell equations [64].

Exact solitons (4) have been found to evolve stably over arbitrarily long distances. However, a defining physical property of a soliton is its robustness against perturbations. Results from numerical simulations are now presented that establish the stability of cubic-quintic Helmholtz solitons. For beams with $\kappa \ll O(1)$ and $\kappa\rho_0 \ll O(1)$, solution (4) has the transverse phase slope,

$$S = V\sqrt{\frac{1+4\kappa\beta}{1+2\kappa V^2}} \simeq \frac{V}{\sqrt{1+2\kappa V^2}} = \frac{\sin\theta}{\sqrt{2\kappa}}.$$

We chose the initial condition

$$u(\xi,0) = \left[\frac{4\beta}{1+\left(1+\frac{4}{3}\alpha\rho_0\right)\cosh(2\sqrt{2\beta}\xi)}\right]^{1/2} \exp(-iS_0\xi), \tag{14}$$

which is an exact solution (12) of the corresponding paraxial equation with transverse velocity S_0. By applying a rotational transformation and examining the beam along its propagation axis [46], it can be seen that the initial condition (14) is equivalent to an on-axis paraxial soliton [17] whose width has been reduced by the Helmholtz factor $(1+2\kappa V^2)^{1/2}$, where $V=S_0(1-2\kappa S_0^2)^{-1/2}$. For a typical value of $\kappa=10^{-3}$ ($\kappa=10^{-4}$), propagation angles of $\theta=15°$, 30°, and 45° occur for $S_0\approx 5.79$ ($S_0\approx 18.30$), $S_0\approx 11.18$ (35.36), and $S_0\approx 15.81$ (=50.00).

Figure 5 shows a typical set of reshaping results for beams with $\alpha=-0.15$. When $\nu=1$, the upper and lower branches on the bistable curve [see Fig. 3(a)] correspond to intensities $\rho_0\simeq 4.14$ and $\rho_0\simeq 1.30$, respectively, while the monostable solution (where $\alpha=+0.15$) has $\rho_0\simeq 0.87$. In all three cases, the parameters (amplitude, width, and area) of the reshaping beam undergo monotonically decreasing oscillations. This type of evolution has been reported for other similarly perturbed Helmholtz solitons, where, typically, the oscillations vanish as $\zeta\to\infty$ to leave a stationary state

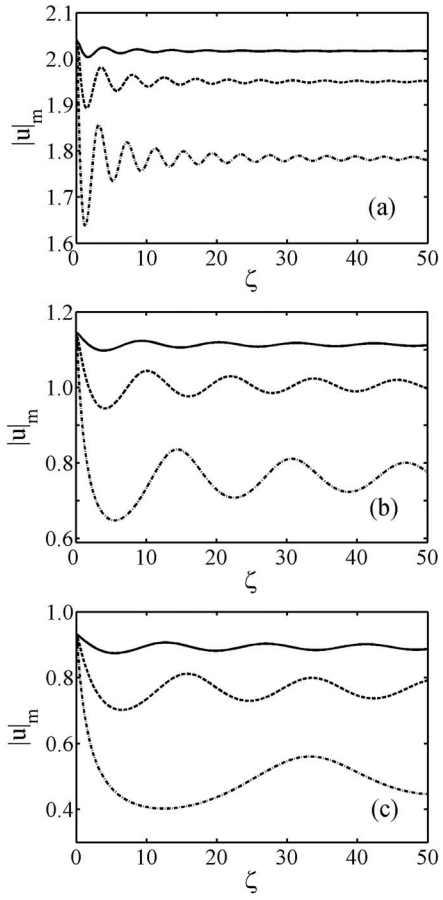

FIG. 5. Reshaping oscillations in the peak amplitude $\sqrt{\rho_0} \equiv |u|_m$ of perturbed bistable solitons (4) with $\alpha=-0.15$, lying on (a) upper, and (b) lower branches of the curve shown in Fig. 3(b). Reshaping of the corresponding monostable soliton (where $\alpha=+0.15$) is shown in part (c). Solid lines: $\theta=15°$; dashed lines: $\theta=30°$; dot-dashed lines: $\theta=45°$.

[48,55–57]. It is interesting to note that for a given $|\alpha|$, the three soliton families (upper branch, lower branch, and monostable) evolve at distinct rates toward their stationary states. Upper-branch solitons have been found to reshape most "rapidly" (with the oscillations occurring over the shortest ζ scale lengths), while the monostable soliton requires the longest distance for the stationary beam to emerge. The same qualitative features have been observed for a wide range of values of $|\alpha|$. By fixing the perturbation S_0 and varying $|\alpha|$, it has been found that increasing $|\alpha|$ leads to slightly "faster" reshaping oscillations.

The evolution of a perturbed soliton in $(|u|_m, \partial_\zeta|u|_m, \zeta)$ space is plotted in Fig. 6(a). The trajectory winds towards an axis that is parallel to the ζ axis, and that passes through $\partial_\zeta|u|_m=0$. In Fig. 6(b), the orbit is projected onto the $(|u|_m, \partial_\zeta|u|_m)$ plane. In this two-dimensional representation, it can be seen that the trajectory is strongly attracted toward a single fixed point. One of the coordinates of this fixed point is always $\partial_\zeta|u|_m=0$, but the precise location of the other coordinate, along the $|u|_m$ axis, depends upon the initial perturbation. In this sense, one can interpret the stationary Helmholtz beam that emerges asymptotically from Eq. (14) as a

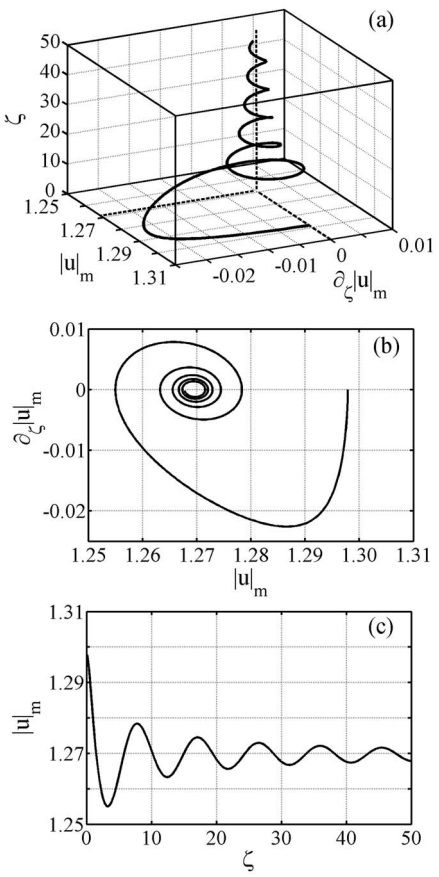

FIG. 6. (a) Evolution of a weakly perturbed lower-branch soliton ($\alpha=-0.2$, $\rho_0\approx 1.68$) in $(|u|_m, \partial_\zeta|u|_m, \zeta)$ space. (b) Projection of the orbit in part (a) onto the $(|u|_m, \partial_\zeta|u|_m)$ plane. (c) Projection of the orbit in part (a) onto the $(\zeta, |u|_m)$ plane. The scale length of the reshaping oscillation is comparable with that shown in Fig. 5(b) (solid line).

fixed-point attractor of the system, in whose basin of attraction the input beam resides. In Fig. 6(c), the orbit is projected onto the $(\zeta, |u|_m)$ plane, revealing the monotonically decreasing oscillations in the peak amplitude. This particular plot also illustrates the character of the curves shown in Fig. 5.

The "fixed-point" classification is based upon a qualitative comparison with classic phase portraits that arise in dissipative dynamical systems [61,65]. Mathematically, Eq. (3) is conservative, and so, strictly, fixed points cannot exist. However, the small amount of radiation that is shed during reshaping can be regarded as a source of *local* dissipation, while energy flow, momentum, and energy [i.e., the integrals in Eqs. (10)] are conserved *globally*. The notion of systems that are locally dissipative and (simultaneously) globally conservative has been discussed in more detail elsewhere [55–57].

V. CONCLUSIONS

We have presented the exact analytical bistable soliton solutions to a nonlinear-Helmholtz governing equation. The structure of the spatially symmetric, cubic-quintic solitons has been explored in detail. It has been shown that geometrical corrections to off-axis beam evolution may be of arbitrary magnitude, and that they are independent of both the system nonlinearity and the inverse beamwidth parameter κ. Well-known paraxial solutions [17] emerge from the more general Helmholtz solitons when a simultaneous multiple limit is enforced. Finally, well-tested numerical analyses have confirmed the robustness of the Helmholtz solitons against perturbations.

The results reported in this work have innate mathematical appeal in the context of generic nonlinear partial differential equations. A generalized analysis has revealed that bistable regimes can always be accessed, irrespective of $|\alpha|$, by varying ν (i.e., by changing the soliton FWHM). We have found that broader beams allow a larger region of bistability, and this finding has particular physical importance. It demonstrates that the character of the bistability depends on the properties of the optical beam itself, rather than on the material parameters. The type of intrinsic bistability that we have studied in this paper is therefore possible (at least in principle) in all cubic-quintic materials with $n_2>0$ and $n_4<0$, regardless of the relative *magnitude* of these coefficients.

We propose that Helmholtz soliton theory provides the ideal platform for the design and modeling of any future optical ICT devices that exploit arbitrary-angle effects with bistable and/or multistable operation. For example, the solutions reported here provide the basis functions for generalizing our recent work on Kerr interface geometries [53] to include cubic-quintic and saturable materials [66] and bistable multibeam contexts [67]. We have also started to analyze how bistable solitons interact in arbitrary-angle regimes [52,57]. These investigations are directly relevant to other areas of very active research, including spatial-soliton dragging [68], logic [69], switching [70,71], and coupled waveguide arrays [72]. Helmholtz solitons offer countless exciting new theoretical challenges and experimental prospects. We expect that new qualitative and quantitative phenomena will be discovered once full account is taken of spatial symmetry in nonlinear optical systems.

[1] Y. S. Kivshar and B. A. Malomed, Rev. Mod. Phys. **61**, 765 (1989).
[2] Y. S. Kivshar, Opt. Quantum Electron. **30**, 571 (1998).
[3] Y. S. Kivshar and B. Luther Davies, Phys. Rep. **298**, 81 (1998).
[4] G. Stegeman and M. Segev, Science **286**, 1518 (1999).
[5] B. Luther-Davies and Y. Xiaoping, Opt. Lett. **17**, 496 (1992).
[6] M. Shalaby and A. Barthelemy, Opt. Lett. **16**, 1472 (1991); T. T. Shi and S. Chi, *ibid.* **15**, 1123 (1990).
[7] X. D. Cao and D. D. Meyerhofer, Opt. Lett. **19**, 1711 (1994).

[8] G. S. McDonald and W. J. Firth, J. Opt. Soc. Am. B **10**, 1081 (1993); **7**, 1328 (1990); J. Mod. Opt. **37**, 613 (1990).
[9] C. Anastassiou, M. Segev, K. Steiglitz, J. A. Giordmaine, M. Mitchell, M. F. Shih, S. Lan, and J. Martin, Phys. Rev. Lett. **83**, 2332 (1999); M. H. Jakubowski, K. Steiglitz, and R. Squier, Phys. Rev. E **58**, 6752 (1998).
[10] A. E. Kaplan, Phys. Rev. Lett. **55**, 1291 (1985).
[11] A. E. Kaplan, IEEE J. Quantum Electron. **QE-21**, 1538 (1985).
[12] R. H. Enns, S. S. Rangnekar, and A. E. Kaplan, Phys. Rev. A **35**, 466 (1987); **36**, 1270 (1987); R. H. Enns and S. S. Rangnekar, Phys. Rev. Lett. **57**, 778 (1986); A. E. Kaplan, *ibid.* **57**, 779 (1986).
[13] L. J. Mulder and R. H. Enns, IEEE J. Quantum Electron. **25**, 2205 (1989).
[14] R. H. Enns and S. Rangnekar, Opt. Lett. **12**, 108 (1987); IEEE J. Quantum Electron. **QE-23**, 1199 (1987).
[15] J. Herrmann, J. Opt. Soc. Am. B **8**, 1507 (1991).
[16] S. Gatz and J. Herrmann, J. Opt. Soc. Am. B **8**, 2296 (1991).
[17] J. Herrmann, Opt. Commun. **87**, 161 (1992); S. Gatz and J. Herrmann, IEEE J. Quantum Electron. **28**, 1732 (1992).
[18] W. Krolikowski and B. Luther-Davies, Opt. Lett. **17**, 1414 (1992); **18**, 188 (1993).
[19] Kh. I. Pushkarov, D. I. Pushkarov, and I. V. Tomov, Opt. Quantum Electron. **11**, 471 (1979); Kh. I. Pushkarov and D. I. Pushkarov, Rep. Math. Phys. **17**, 37 (1980).
[20] S. Tanev and D. I. Pushkarov, Opt. Commun. **141**, 322 (1997).
[21] L. H. Acioli, A. S. L. Gomes, J. M. Hickmann, and C. B. de Araujo, Appl. Phys. Lett. **56**, 2279 (1990).
[22] P. Roussignol, D. Ricard, J. Lukasik, and C. Flytzanis, J. Opt. Soc. Am. B **4**, 5 (1987).
[23] B. L. Lawrence and G. I. Stegeman, Opt. Lett. **23**, 591 (1998).
[24] B. L. Lawrence, M. Cha, W. E. Torruellas, G. I. Stegeman, S. Etemad, G. Baker, and F. Kajzar, Appl. Phys. Lett. **64**, 2773 (1994).
[25] B. Lawrence, W. E. Torruellas, M. Cha, M. L. Sundheimer, G. I. Stegeman, J. Meth, S. Etemad, and G. Baker, Phys. Rev. Lett. **73**, 597 (1994).
[26] K. Ogusu, J. Yamasaki, S. Maeda, M. Kitao, and M. Minakata, Opt. Lett. **29**, 265 (2004).
[27] G. Boudebs, S. Cherukulappurath, H. Leblond, J. Troles, F. Smektala, and F. Sanchez, Opt. Commun. **219**, 427 (2003).
[28] F. Smektala, C. Quemard, V. Couderc, and A. Barthélémy, J. Non-Cryst. Solids **274**, 232 (2000).
[29] C. Zhan, D. Zhang, D. Zhu, D. Wang, Y. Li, Z. Lu, L. Zhao, and Y. Nie, J. Opt. Soc. Am. B **19**, 369 (2002).
[30] B. A. Malomed, D. Mihalache, F. Wise, and L. Torner, J. Opt. B: Quantum Semiclassical Opt. **7**, R53 (2005).
[31] S. Gatz and J. Herrmann, Opt. Lett. **17**, 484 (1992).
[32] L. Coutaz and M. Kull, J. Opt. Soc. Am. B **8**, 99 (1991).
[33] M. Lax, W. H. Louisell, and W. B. McKnight, Phys. Rev. A **11**, 1365 (1975).
[34] S. Chi and Q. Guo, Opt. Lett. **20**, 1598 (1995).
[35] A. Ciattoni, B. Crosignani, P. Di Porto, J. Scheuer, and A. Yariv, Opt. Express **14**, 5517 (2006).
[36] A. Ciattoni, B. Crosignani, S. Mookherjea, and A. Yariv, Opt. Lett. **30**, 516 (2005).
[37] B. Crosignani, A. Yariv, and S. Mookherjea, Opt. Lett. **29**, 1524 (2004).
[38] A. Ciattoni, P. Di Porto, B. Crosignani, and A. Yariv, J. Opt. Soc. Am. B **17**, 809 (2000).
[39] E. Granot, S. Stenklar, Y. Isbi, B. A. Malomed, and A. Lewis, Opt. Lett. **22**, 1290 (1997).
[40] E. Granot, S. Sternklar, Y. Isbi, B. Malomed, and A. Lewis, Opt. Commun. **166**, 121 (1999).
[41] E. Granot, S. Sternklar, Y. Isbi, B. A. Malomed, and A. Lewis, Opt. Commun. **178**, 431 (2000).
[42] B. V. Gisin and B. A. Malomed, J. Opt. A, Pure Appl. Opt. **3**, 284 (2001).
[43] B. A. Malomed, K. Marinov, D. I. Pushkarov, and A. Shivarova, Phys. Rev. A **64**, 023814 (2001).
[44] B. V. Gisin and B. A. Malomed, J. Opt. Soc. Am. B **18**, 1356 (2001).
[45] P. Chamorro-Posada, G. S. McDonald, and G. H. C. New, J. Mod. Opt. **45**, 1111 (1998).
[46] P. Chamorro-Posada, G. S. McDonald, and G. H. C. New, J. Opt. Soc. Am. B **19**, 1216 (2002).
[47] J. M. Christian, G. S. McDonald, and P. Chamorro-Posada, Phys. Rev. E **74**, 066612 (2006).
[48] P. Chamorro-Posada, G. S. McDonald, and G. H. C. New, J. Mod. Opt. **47**, 1877 (2000).
[49] M. D. Feit and J. A. Fleck, J. Opt. Soc. Am. B **5**, 633 (1988).
[50] J. P. Gordon, Opt. Lett. **8**, 596 (1983); O. Cohen, R. Uzdin, T. Carmon, J. W. Fleischer, M. Segev, and S. Odoulov, Phys. Rev. Lett. **89**, 133901 (2002).
[51] A. B. Aceves, J. V. Moloney, and A. C. Newell, Phys. Rev. A **39**, 1809 (1989); **39**, 1828 (1989).
[52] P. Chamorro-Posada and G. S. McDonald, Phys. Rev. E **74**, 036609 (2006).
[53] J. Sánchez-Curto, P. Chamorro-Posada, and G. S. McDonald, Opt. Lett. **32**, 1126 (2007).
[54] P. Chamorro-Posada and G. S. McDonald, Opt. Lett. **28**, 825 (2003).
[55] J. M. Christian, G. S. McDonald, and P. Chamorro-Posada, J. Phys. A: Math. Theor. **40**, 1545 (2007); **40**, 8601 (2007).
[56] J. M. Christian, G. S. McDonald, R. J. Potton, and P. Chamorro-Posada, Phys. Rev. A **76**, 033834 (2007).
[57] J. M. Christian, Ph.D. thesis, University of Salford, U.K., 2006.
[58] D. E. Pelinovsky, V. V. Afanasjev, and Y. S. Kivshar, Phys. Rev. E **53**, 1940 (1996).
[59] V. I. Karpman and V. V. Solov'ev, Physica D **3**, 142 (1981).
[60] S. Blair, Chaos **10**, 570 (2000).
[61] H. Goldstein, *Classical Mechanics*, 2nd ed. (Addison Wesley, Philippines, 1980).
[62] P. Chamorro-Posada, G. S. McDonald, and G. H. C. New, Opt. Commun. **192**, 1 (2001).
[63] N. Akhmediev, A. Ankiewicz, and R. Grimshaw, Phys. Rev. E **59**, 6088 (1999).
[64] P. Chamorro-Posada, J. Sánchez-Curto, J. M. Christian, and G. S. McDonald, in Proceedings of the 2nd International Conference on Advanced Optoelectronics and Lasers Vol. II, IEEE, Yalta, 12–17 September, 2005, pp. 108–112.
[65] C. Zhou, X. T. He, and S. Chen, Phys. Rev. A **46**, 2277 (1992).
[66] D. Mihalache, D. Mazilu, M. Bertolotti, and C. Sibilia, J. Opt. Soc. Am. B **5**, 565 (1988).
[67] J. Scheuer and M. Orenstein, Opt. Lett. **24**, 1735 (1999).
[68] J. U. Kang, G. I. Stegeman, A. Villeneuve, and J. S. Aitchison, Pure Appl. Opt. **5**, 583 (1996); J. U. Kang, G. I. Stegeman, and J. S. Aitchison, Opt. Lett. **21**, 189 (1996); S. Blair and K.

Wagner, *ibid.* **19**, 1943 (1994).
[69] S. Blair and K. Wagner, Appl. Opt. **39**, 6006 (2000); **38**, 6749 (1999).
[70] Y. W. Wu, Opt. Express **14**, 4005 (2006); Appl. Opt. **44**, 4144 (2005); Fiber Integr. Opt. **23**, 387 (2004).
[71] F. Garzia, C. Sibilia, and M. Bertolotti, J. Lightwave Technol. **19**, 1036 (2001).
[72] Y. V. Kartashov, A. S. Zelenina, L. Torner, and V. A. Vysloukh, Opt. Lett. **29**, 766 (2004).